Materials Research Proceedings 44 (2024) 597-605 https://doi.org/10.21741/9781644903254-64

Integrating Numerical and experimental analyses for the realization of pre-detection of delayed fractures on punched surfaces of ultra-high-strength steel sheets

UEDA Yuya[1,a], EGUCHI Jin[1,b], and MATSUNO Takashi[1,c *]

[1]Faculty of Engineering, Tottori University 4-101 Koyama-cho-minami, Tottori-city, Tottori 680-8552, Japan

[a]yuya.flower0307@gmail.com, [b]vintagejkj@gmail.com, [c]matsu@tottori-u.ac.jp

Keywords: Punching, Finite Element Simulation, Residual Stress

Abstract. A key challenge encountered in finite element (FE) punching simulations is accurately capturing the arrest or delay in crack propagation during punch penetration. Conventional methods relying on element deletion demonstrate inadequacies in representing crack arrest, particularly complicating the simulation of the punched surface states in scenarios with minute clearances. This study introduces a novel approach for fracture representation in FE punching simulations, wherein cracks were integrated as perimeter lines during the remeshing process. Utilizing observation-driven crack propagation paths and arrest behaviors, we analyzed the residual stress on punched surfaces under minimal clearance conditions. Results indicate that for 22MnB5 hot-stamped steel, the residual stresses within the interior side of the burnished region can exceed 1 GPa in cases with a 10-μm clearance.

Introduction

Punched surfaces of ultra-high-strength steel sheets (UHSSs) exhibit significant residual tensile stresses [1, 2] and reduced ductility compared to their as-received conditions [3]. Consequently, in automotive applications, concerns arise as the tensile strength of UHSSs exceeds 1.5 GPa, leading to increased apprehensions regarding delayed fractures induced by hydrogen embrittlement on punched surfaces [1, 2, 4]. When conventional punch-die clearances surpass 10%t, where %t represents the ratio of the clearance relative to the sheet thickness, these delayed fractures can be attributed to pronounced tensile residual stresses on the punched surfaces [1, 2, 4]. The process of actual press forming emphasizes monitoring the potential for delayed fractures and comprehending the associated residual stress on the punched edges.

Matsuno et al. [5] revealed that delayed fractures are absent in die-quenched steel sheets with a tensile strength of 1.5 GPa on punched surfaces with minute clearances of less than 10 μm. The prevailing theory posits that this absence results from the compressive residual stress applied to the burnishing process within these minute clearances. However, another report have suggested that UHSSs may exhibit tensile residual stresses within the burnished surfaces [6], introducing ambiguity about the definitive influence of the compressive residual stress at such minute clearances.

Finite element (FE) simulations are crucial for assessing residual stress on punched surfaces, yet they encounter obstacles in accurately capturing the fracture process in cases involving minute clearances and repeated crack progression and arrest. Currently, a ductile fracture model applicable to such conditions of compression has not been sufficiently formulated. Our group endeavored to inversely derive ductile fracture loci from FE punching simulations [7], revealing that the shapes of the identified ductile fracture loci (design curves) significantly deviate from those traditionally recognized. Moreover, in several commercially available FE codes that employ the element deletion technique, fractures invariably propagate instantly through the entire sheet thickness

without pausing, due to the inability of these codes to replicate crack arresting behavior that leads to the formation of secondary burnished zones [8].

In this study, a FE punching simulation employing a crack line update method [9] is introduced. This method, distinctively devoid of ductile fracture loci, heuristically updates crack lines to closely mimic the actual observed profile of the punched surface. Simulations performed on quenched 22MnB5 steel sheets with a minute clearance of 10 μm revealed an internal residual stress distribution exceeding 1 GPa. Such elevated stress levels are posited as a potential cause for delayed fractures on punched surfaces. Intriguingly, punched holes in this study exhibited delayed fractures under bending conditions, even though JSC1180Y steel, boasting a tensile strength of 1180 MPa, previously showed no signs of delayed fractures on surfaces punched with similar minute clearance [5].

Material

The test material was a quenched 22MnB5 steel sheet employed in the automobile hot-stamping process, whose mechanical properties are detailed in Table 1. The tensile strength of this material surpasses 1.5 GPa.

Table 1. Mechanical properties of 22MnB5.

Yield stress [MPa]	Tensile strength [MPa]	Uniform elongation [%]	Total elongation [%]
951.4	1600.9	4.78	7.19

For the shearing simulation, the flow stress curve within the large deformation region must be established. Consequently, this study employed a real-time diameter measurement type tensile test combined with FE simulation [10-12] to acquire the flow stress curve extending to fracture. The stress curve was characterized by the modified Swift law [10-12] as follows:

$$Y(\bar{\varepsilon}_p) = (1-a)Y_s(\bar{\varepsilon}_p) + a\{Y_l(\bar{\varepsilon}_p) - 7.134\}, \quad (1)$$

where

$$Y_s(\bar{\varepsilon}_p) = 1672(\bar{\varepsilon}_p + 1.460 \times 10^{-3})^{0.06}, \quad (2)$$

$$Y_l(\bar{\varepsilon}_p) = 1574(\bar{\varepsilon}_p + 2.503 \times 10^{-4})^{0.04}, \quad (3)$$

$$a = 0.5\{\tanh(10(\bar{\varepsilon}_p - 0.06)) + 1\}. \quad (4)$$

In Eq. 1, $Y_s(\bar{\varepsilon}_p)$ represents the Swift work-hardening law for the lower strain region, while $Y_l(\bar{\varepsilon}_p)$ represents the Swift work-hardening law for the larger strain region. For the yield stress $Y(\bar{\varepsilon}_p)$ in the modified Swift law, $Y_s(\bar{\varepsilon}_p)$ and $Y_l(\bar{\varepsilon}_p)$ are smoothly connected at an equivalent plastic strain $\overline{\varepsilon}_p$ of 0.06 using a switching function a.

Shearing simulation with crack-line update method

This analysis was performed using the commercial Abaqus/Standard FE software. Fig. 1 illustrates the FE model configured for the shearing simulation. The specimen was modeled using axisymmetric two-dimensional (2D) quadrilateral elements. In regions undergoing substantial deformation, a dense mesh with an element side length of 0.0025 mm was applied, while other

areas were meshed with the larger size of 0.2 mm. The punch and die edges were modeled with 0.02 mm radii. The clearance between the punch and die was 0.8%t.

A remeshing sequence was deemed essential for the accuracy of the shearing simulation owing to the significantly large expected strain, which could lead to element distortion. Accordingly, remeshing was performed at each increment of 0.01 mm of punch penetration to maintain the integrity of the mesh throughout the simulation process.

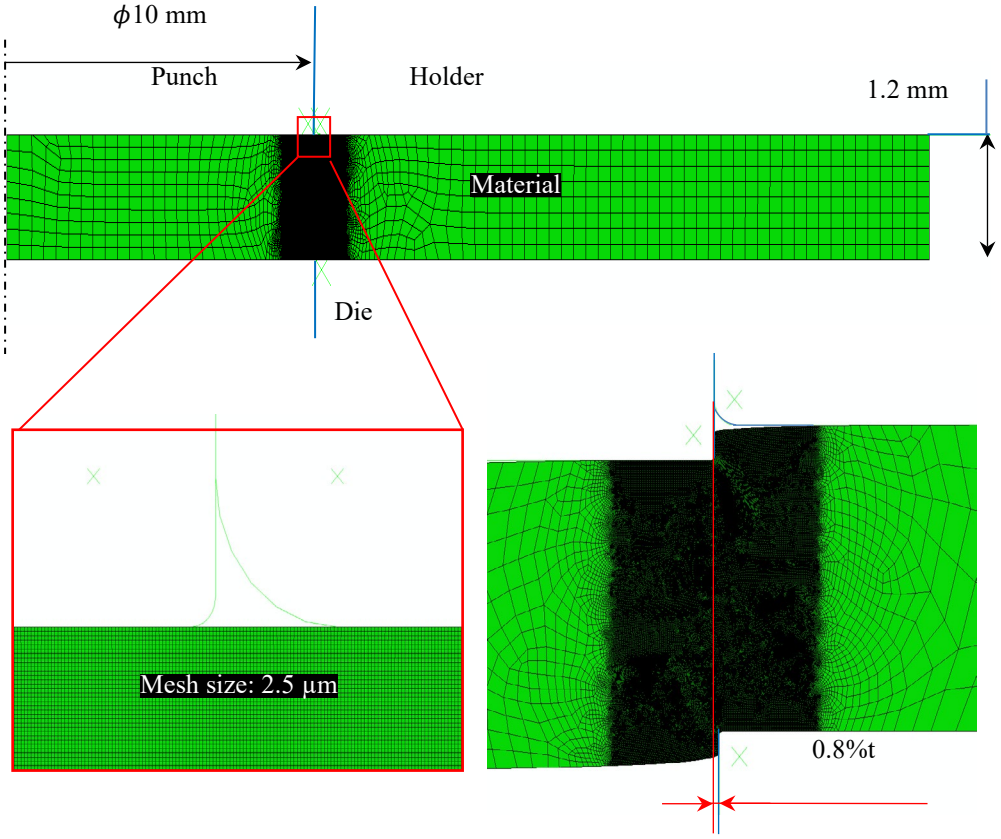

Fig. 1. Boundary conditions and initial meshes for punching simulation.

A notable aspect of this study is the strategic addition of crack lines originating close to the edges of the punch and die. These crack lines were systematically updated along the periphery of the workpiece with each remeshing sequence, as illustrated in Fig. 2. This technique, designated as the "crack-line update method," [9] is a key feature of our simulation approach.

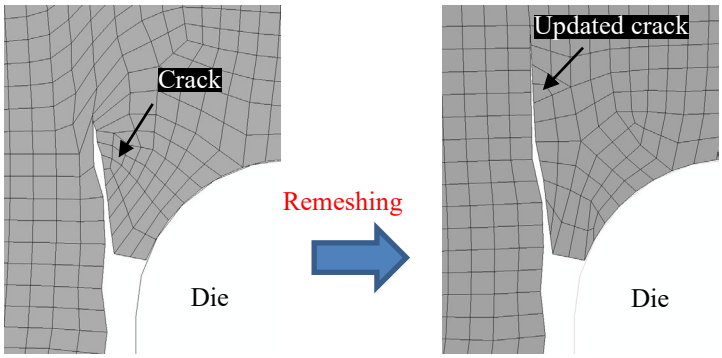

Fig. 2. Fracture expression in FE simulation with crack-line update method.

Assimilation approach for crack-line update method

We devised an assimilation technique precisely capturing the actual profile of the fracture zone observed on the cross-section of punched specimens in our residual stress analysis, separate from prediction methodologies. Fig. 3 illustrates the observation of the actual punched surface for this analysis, with the reference profile derived from the cross-section (Fig. 3(a)). This technique mandated periodic updates to the crack lines to accurately mirror the progression of observed fractures, emulating the fracture zone profile.

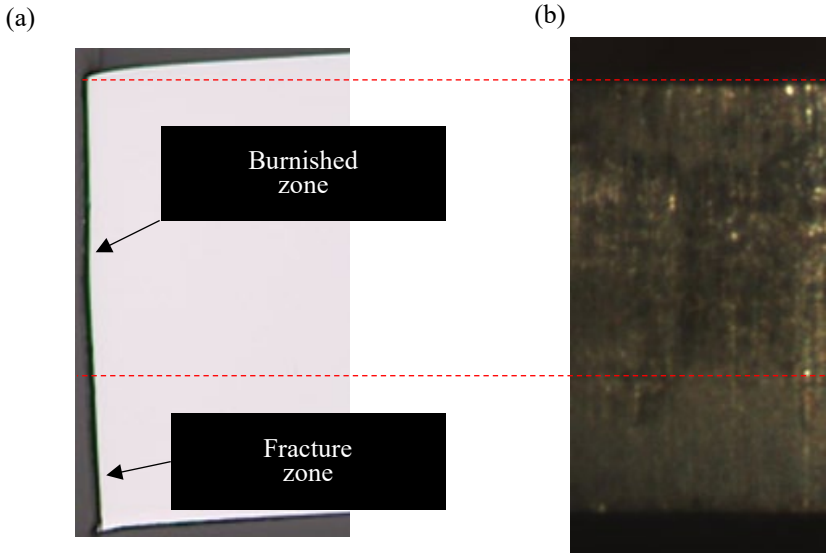

Fig. 3. Observation of punched surface. (a) Cross-section view, (b) Front view.

The progression of these crack lines was determined using empirical data from half-punched specimens, as depicted in Fig. 4. Notably, no cracks are observed around the punch edges. Consequently, only the cracks initiated around the die edge were included in the FE simulation. Internal cracks, such as those in Fig. 4, were omitted from evaluating crack length, considering their origin from propagation in the circumferential direction around the hole, distinct from the assessed primary crack growth.

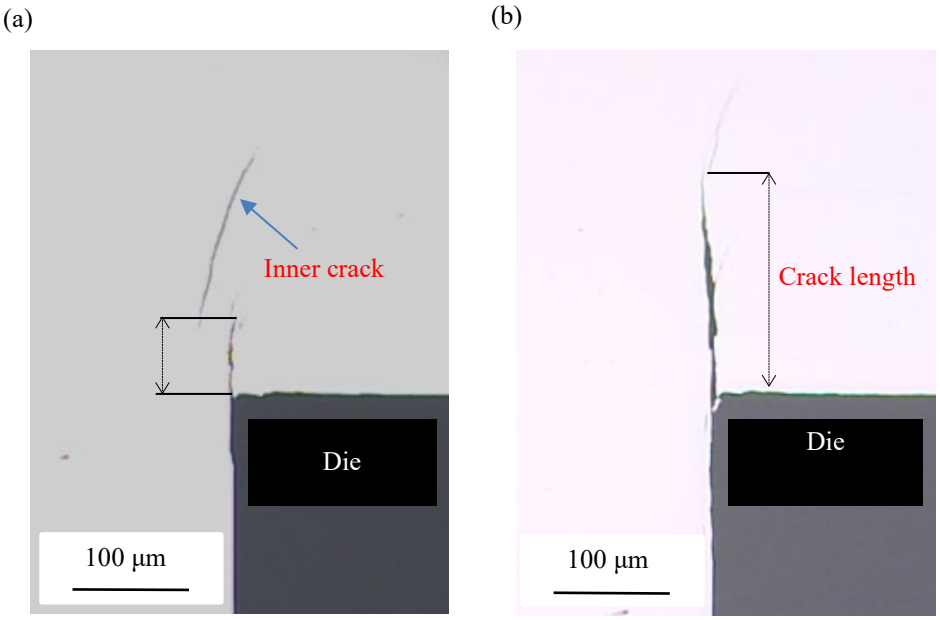

Fig. 4. Cracks observed on the cross-section of a half-punched specimen: punch penetration of (a) 0.24 mm and (b) 0.36 mm.

Fig. 5 demonstrates a linear correlation between crack length and punch penetration up to a 0.6 mm threshold. Beyond this penetration depth, the crack growth pattern became erratic, with non-uniform expansion around the circumference of the hole. Importantly, some specimens, subjected to punch penetrations beyond 0.6 mm, fractured during preparation, indicating complete crack penetration. These half-punched specimens contributed only to the incremental extension of crack length, not determining the directionality of crack-line updates.

Observational crack-propagation uncertainty implies variability in crack length due to crack arrest phenomena, particularly prevalent under conditions of minute clearance. Consequently, certain approximations were necessary when defining the additional crack length in each update sequence to integrate the observed crack progression into our simulation accurately.

This study performed crack-length determination through two different approaches. The first approach envisioned cracks growing continuously and uninterrupted, providing a clear view of progression without the complexities of arrest. This method used the correlation between punch penetration and crack length (Fig. 5) to determine crack lengths through linear interpolation. The second approach adopted a more nuanced view by incorporating the concept of crack arrest, which was achieved by introducing stopping points in crack growth rather than a straightforward linear interpolation.

In the second approach, the update sequence for the crack lines paused when the propagation trajectory approached the boundary defined by the punch-die clearance space. In the first approach, crack lines tended to follow the material surfaces as they rotated because of punch penetration, often causing them to extend beyond the designated clearance area. Hence, a crack-arrest sequence was employed in the second approach for its proactive prevention. Following the arrest phase, the crack lines were updated to align with the punch penetration and crack length relationship, as depicted in Fig. 5. This process resulted in the arrest of crack-line propagation within the steps corresponding to punch penetration increasing from 0.37 mm to 0.76 mm, an effective increment of 0.31 mm. When the punch penetration reached 0.76 mm, the material completely separated.

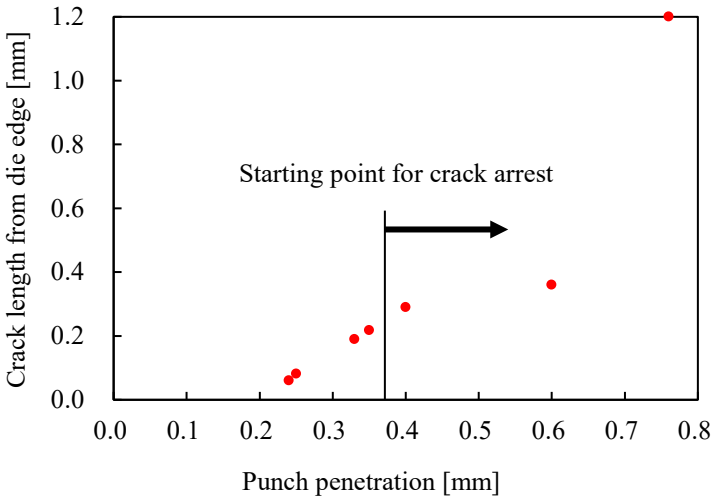

Fig. 5. Relationship between crack length and punch penetration for half-punched specimens.

Results and discussion

Fig. 6 depicts the FE simulations (circumferential stress map) with the actual cross-sectional image. Fig. 6(a) represents the case without crack arrest, while Fig. 6(b) represents the case with crack arrest.

A significant deviation from the actual cross-sectional profile is observed in the simulation case without crack arrest (Fig. 6(a)). A large and irregular protrusion is formed due to the orientation of crack lines during punch penetration. Without crack arrest, the cracks excessively expand, deviating from the clearance region and extending into the interior of the punch side. The deviated crack is subsequently pressed by the punch and rotated along the direction of punch penetration, resulting in an abnormal protrusion. This protrusion significantly influences the residual stress distribution, inducing a compressive stress state around it. It leads to high tensile residual stress in the burnished region as a response to the localized compressive stress concentration.

Conversely, when crack arrest is incorporated into the simulation (Fig. 6(b)), protrusion formation is notably absent, resulting in a closer approximation of the actual punched surface profile. However, the simulation did not completely replicate the effects of an insufficient blank holder force, resulting in a slight discrepancy between the simulated and actual raised punched surface profiles. Therefore, the simulation provided a significant first step in understanding cases with minute clearances. Particularly notable was the simulation revelation of tensile stresses exceeding 1 GPa in the interior of the burnished zone, contrasting sharply with the low or compressive stresses on the surface, providing crucial insights for delayed fracture analysis. This outcome emphasizes the need for further investigations into the mechanisms governing such stress distributions, which are crucial for predicting the service life of punched components.

To validate the circumferential residual stress as numerically simulated in the FE analyses, an X-ray diffraction (XRD) measurement was conducted at the center of the punched surface. This measurement was performed using a μ360s instrument (Pulstec Industry Co., Ltd.) equipped with a 0.8-mm beam spot and 0.5-mm collimator size; it yielded a circumferential residual stress of -149 MPa. The circumferential stress simulated in the case with crack arrest was approximately 10 MPa, averaged over the corresponding surface area in alignment with the measurement.

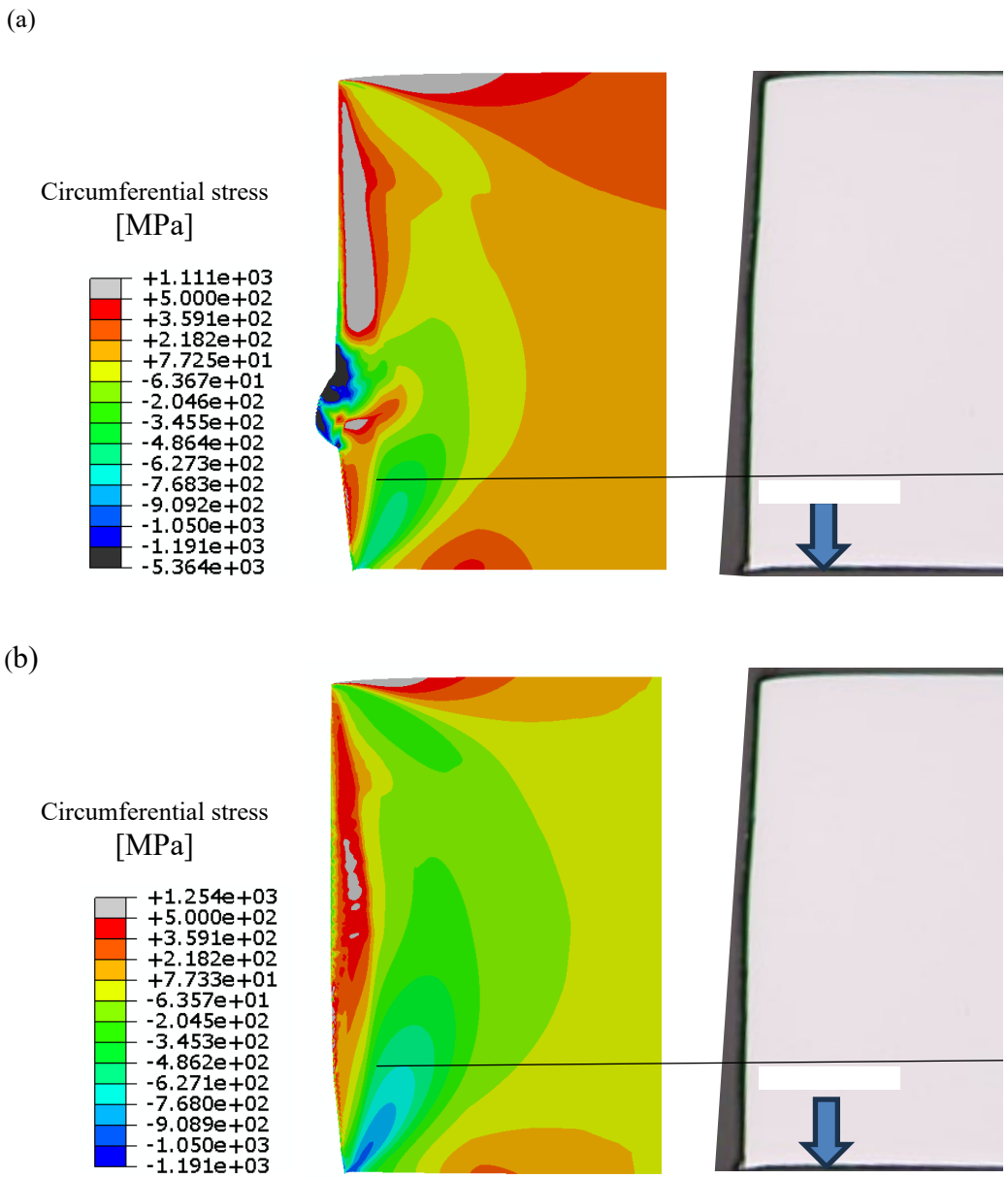

Fig. 6. Circumferential residual stress FE-simulated with crack-line update method. The actual punched surface shown in Fig. 3 is also shown for reference. (a) Case without crack arrest, (b) Case with crack arrest.

The simulation indicated higher residual stress levels than the actual measurements. This discrepancy can be largely attributed to the flattening process designed to eliminate concavities during the creation of the burnished zone [8]. The simulated residual stresses were considered valid despite this error source. This is particularly true because the high tensile residual stresses, critical for actual delayed fracture, were broadly distributed and more pronounced. Essentially, the localized residual stress near the surface was found to have a limited impact. As our methodology advanced, the precision of replicating the fracture surface improved significantly, enhancing the accuracy of the residual stress distribution analysis.

The validation of the FE-simulated stresses in the thickness direction remained underexplored in our study, primarily due to the significant scattering observed in XRD measurements of residual stress. This variability constrained our ability to validate the analytical results related to this aspect

robustly. Consequently, we present our stress distribution analysis outcomes in Fig. 7 as illustrative data rather than definitive conclusions.

A notable concentration of compressive stress is evident around the protrusion in the absence of crack arrest (see Fig. 7(a)). This phenomenon is attributed to the residual stress induced by the punch penetration, persisting in the affected area. Conversely, such pronounced compressive stresses are not observed with crack arrest owing to the absence of protrusions (Fig. 7(b)). The punched surface generally exhibits compressive or low-tensile residual stress, excluding the protrusion region. Notably, residual tensile stresses ranging from 200 to 300 MPa are detected in certain areas within the burnished zone. The precision of this analysis warrants further investigation, presenting an area for future research.

Simulating crack progression exclusively from the die side and subsequent residual stress analysis was challenging due to the absence of established ductile fracture criteria under low or negative stress triaxiality conditions. Typically, punch-side cracking was inevitable in FE simulations using conventional ductile fracture loci. However, the proposed assimilation method facilitates such analyses without relying on a ductile fracture model. This significant advancement is the primary focus of our rapid publication.

In the future, we aim to further refine our assimilation technique by incorporating actual punched surface irregularities, such as surface tilting and extensive burr formation, to improve the fidelity of the simulation to real-world conditions.

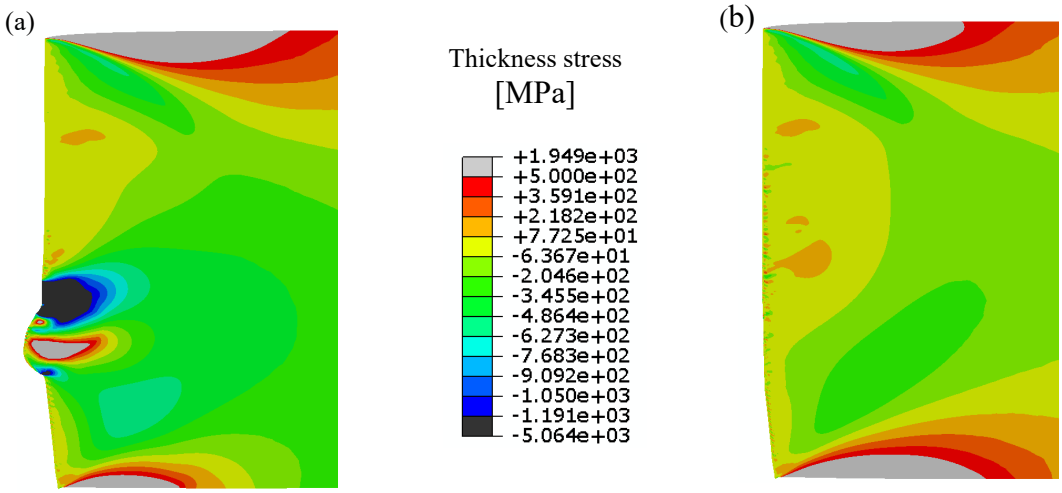

Fig. 7. Comparison of thickness stress with and without crack arrest. (a) Without crack arrest, (b) With crack arrest.

Conclusion

In this study, we introduced a FE simulation technique capable of accurately replicating the punched surface profile of hot-stamped 22MnB5 UHSS without utilizing a damage model. This approach allowed successful visualization of residual stresses in cases of minute clearance.

During the FE simulations, straightforward linear interpolation of crack propagation behavior led to the development of a protrusion on the punched surface. Consequently, the residual stress analyzed in this case differed from the actual residual stress observed on the punched surface. Nevertheless, by implementing a crack arrest strategy, we were able to prevent the formation of this protrusion. The residual stresses determined were in close agreement with empirical measurements. Future efforts should focus on further refining the replication of crack halting behavior, as well as integrating considerations of ductile fracture models.

The insights gained from this study contribute to the broader discussion on the delayed fracture stress threshold of punched surfaces in UHSSs, augmenting separate investigations into delayed fractures on punched surfaces carried out by the authors. To gain a more comprehensive

understanding of the findings of this paper, readers are encouraged to consult our previous publications.

References

[1] K.-i. Mori, Y. Abe, K. Sedoguchi, Delayed fracture in cold blanking of ultra-high strength steel sheets, CIRP Annals, 68 (2019) 297-300. https://doi.org/10.1016/j.cirp.2019.04.111

[2] T. Matsuno, Y. Sekito, E. Sakurada, T. Suzuki, K. Kawasaki, M. Suehiro, Resistance of hydrogen embrittlement on hot-sheared surface during die-quench process, ISIJ Int. 54 (2014) 2369-2374. https://doi.org/10.2355/isijinternational.54.2369

[3] T. Matsuno, N. Kinoshita, T. Matsuda, Y. Honda, T. Yasutomi, Microvoid formation of ferrite-martensite dual-phase steel via tensile deformation after severe plastic shear-deformation, ISIJ Int. 63 (2023) 941-949. https://doi.org/10.2355/isijinternational.ISIJINT-2023-012

[4] M. Yoshino, Y. Toji, S. Takagi, K. Hasegawa, Influence of sheared edge on hydrogen embrittlement resistance in an ultra-high strength steel sheet, ISIJ Int. 54 (2014) 1416-1425. https://doi.org/10.2355/isijinternational.54.1416

[5] T. Matsuno, Y. Ueda, T. Takahashi, T. Hama, T. Hojo, Y. Shibayama, M. Ridha, Y. Okitsu, M. Takamura, Delayed fracture stress thresholds degraded by shear punching process in ultra-high-strength steel sheets: Analysis using an in-plane bending test with numerical assimilation, J. Manuf. Process. 119 (2024) 1005-1021. https://doi.org/10.1016/j.jmapro.2024.04.013

[6] T. Matsuno, Y. Ochiai, Y. Okitsu, M. Iga, A. Kohri, T. Mikami, Surface and interior residual stress analysis of a deep-drawn 1180-MPa class ultra-high strength steel sheet with scratch marks, Int. J. Adv. Manuf. Tech. 116 (2021) 2873-2884. https://doi.org/10.1007/s00170-021-07675-2

[7] T. Matsuno, K. Nakagiri, T. Matsuda, T. Tanaka, T. Yasutomi, H. Shoji, M. Ohata, Identification of ductile fracture design curve for hardened quasi-brittle AISI-D2 tool steel to predict shearing tool failure, J. Mater. Process. Tech. 307 (2022). https://doi.org/10.1016/j.jmatprotec.2022.117680

[8] T. Matsuno, A. Seto, M. Suehiro, Y. Kuriyama, H. Murakami, FEM analysis of high strength steel sheets up to fracture and its application to piercing process, Proceedings of IDDRG2012, (2012) 134-140.

[9] T. Matsuno, M. Takamura, S. Mihara, T. Koda, K. Tsujioka, Development of the crack-line-update method for two-dimensional piercing simulations, Journal of Physics: Conference Series, 1063 (2018) 012157. https://doi.org/10.1088/1742-6596/1063/1/012157

[10] T. Matsuno, T. Fujita, T. Matsuda, Y. Shibayama, T. Hojo, I. Watanabe, Unstable stress-triaxiality development and contrasting weakening in two types of high-strength transformation-induced plasticity(TRIP) steels: Insights from a new compact tensile testing method, J. Mater. Process. Tech. 322 (2023) 118174. https://doi.org/10.1016/j.jmatprotec.2023.118174

[11] T. Matsuno, D. Kondo, T. Hama, T. Naito, Y. Okitsu, S. Hayashi, K. Takada, Flow stress curves for 980MPa- and 1.5GPa-class ultra-high-strength steel sheets weakened under high-stress triaxiality, Int. J. Mech. Sci. 261 (2024) 108671. https://doi.org/10.1016/j.ijmecsci.2023.108671

[12] T. Matsuno, T. Hojo, I. Watanabe, A. Shiro, T. Shobu, K. Kajiwara, Tensile deformation behavior of TRIP-aided bainitic ferrite steel in the post-necking strain region, Sci. Tech. Adv. Mater.: Methods 1 (2021) 56-74. https://doi.org/10.1080/27660400.2021.1922207